# Wet Catalyst-Support Films for Production of Vertically Aligned Carbon Nanotubes

Noe T. Alvarez,[†,‡] Christopher E. Hamilton,[†,‡] Cary L. Pint,[‡,§] Alvin Orbaek,[†,‡] Jun Yao,[‡,⊥] Aldo L. Frosinini,[‡] Andrew R. Barron,[*,†,‡,∥] James M. Tour,[*,†,‡,∥] and Robert H. Hauge[*,†,‡]

Departments of Chemistry, The Richard E. Smalley Institute for Nanoscale Science and Technology, Department of Physics and Astronomy, Applied Physics Program through the Department of Bioengineering, and Department of Mechanical Engineering and Materials Science, Rice University, MS 222, 6100 Main Street, Houston, Texas 77005

**ABSTRACT** A procedure for vertically aligned carbon nanotube (VA-CNT) production has been developed through liquid-phase deposition of alumoxanes (aluminum oxide hydroxides, boehmite) as a catalyst support. Through a simple spin-coating of alumoxane nanoparticles, uniform centimer-square thin film surfaces were coated and used as supports for subsequent deposition of metal catalyst. Uniform VA-CNTs are observed to grow from this film following deposition of both conventional evaporated Fe catalyst, as well as premade Fe nanoparticles drop-dried from the liquid phase. The quality and uniformity of the VA-CNTs are comparable to growth from conventional evaporated layers of $Al_2O_3$. The combined use of alumoxane and Fe nanoparticles to coat surfaces represents an inexpensive and scalable approach to large-scale VA-CNT production that makes chemical vapor deposition significantly more competitive when compared to other CNT production techniques.

**KEYWORDS:** vertically aligned carbon nanotubes • alumoxane • catalyst support • chemical vapor deposition

## INTRODUCTION

Since their discovery, carbon nanotubes (CNTs) have captivated the field of nanotechnology. Their unique structure, size, and physical properties (1, 2) makes them premier candidates for a broad range of applications, ranging from electronics to energy storage devices (3−9). Although not all the reported applications will require large-scale CNT usage, there are applications where large volumes of CNTs will be required, such as in fiber-composites, films, coatings, and additives. As a result, the necessity exists for large-scale and inexpensive approaches to produce carbon nanotubes. One of the most important aspects limiting the integration of CNTs into applications to displace conventional bulk materials is the cost of both production and processing of CNTs. In the first case, there is a broad effort to boost production of CNTs using scaled-up processes of existing techniques, or the development of new cost-effective approaches. Various techniques for CNT growth which have potential for mass production have been developed, including the HiPco (10), fluidized bed (11−14), and chemical vapor deposition (CVD) (15−17) methods. Concurrently, the ability to grow vertically aligned carbon nanotubes (VA-CNTs) offers a new approach to large-scale production, with the as-grown structure composed of long, well-aligned CNTs (17). Although VA-CNT growth reduces or eliminates the necessary postgrowth processing of the CNTs, it is normally strongly dependent on the use of expensive substrate materials and deposition equipment that limits the potential for scaling this approach. However, as described here, a wet chemical approach provides an inexpensive and scalable catalyst and catalyst support layer for this growth and it will likely play a key role in defining the cost and the availability of aligned CNTs in the future and could strongly impact the market for applications based on VA-CNTs (18, 19).

In comparison to the traditional synthetic methods for CNT growth, CVD growth offers significant benefits with regard to large scale, low-cost CNT production. The simplicity of parameter control, its suitability for growth on large (wafer-scale) and irregular substrates and the wide range of catalysts possible are all benefits compared to competing methodologies. Although the continuous, scaled-up production of VA-CNTs has not yet been demonstrated, factors relevant to this concept have been the focus of many research efforts. Recent work has shown that roll-to-roll e-beam deposition can be used to form flakes composed of the catalyst and catalyst support which can produce high yields of VA-CNTs without the necessity of a substrate under the catalyst support (20), whereas others, using traditional sputtering and increasing the reactor dimensions, were able to produce 8 in. wafers of VA-CNT (17). Other studies have investigated perturbations to the conventional wafer-support growth technique, focusing on catalyst deposition methods, multicomponent catalyst materials (incorporating Fe, Co, and Ni), and new substrates and catalyst supports to aid and assist the growth process (21). Along these lines, alternative procedures for catalyst deposition have been demonstrated, including nanoparticle spin-coating (22, 23), dip-coating (24),

* Corresponding author. E-mail: tour@rice.edu (J.M.T.); hauge@rice.edu (R.H.H.); arb@rice.edu (A.R.B.).
Received for review February 12, 2010 and accepted May 17, 2010
† Departments of Chemistry, Rice University.
‡ The Richard E. Smalley Institute for Nanoscale Science, Rice University.
§ Department of Physics and Astronomy, Rice University.
∥ Department of Mechanical Engineering and Materials Science, Rice University.
⊥ Applied Physics Program through the Department of Bioengineering.
DOI: 10.1021/am100128m

**Scheme 1. Illustration of the Alumoxane Nanoparticle Processing, Deposition As Thin Films of Catalyst Support Deposition and VA-CNTs Grown from Evaporated Fe Catalyst As Well As Premade Fe Catalyst Nanoparticles**

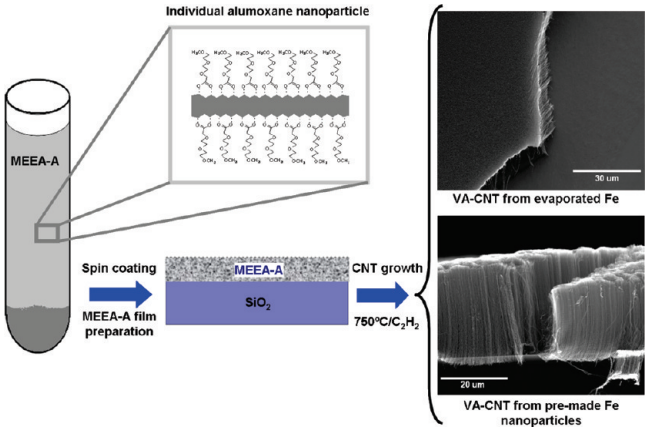


sol−gel (25), and layer by layer metal deposition (26). However, for good-quality VA-CNT growth, these techniques still require conventional $Al_2O_3$ coating via e-beam deposition or sputtering. Several studies have been performed to overcome this difficulty by using different supporting substrates for CNT growth which include zeolites (27), metal oxides (28), sapphire (29), quartz (30), and inexpensive metal foils (31, 32). In addition, alumina particles have been used in the past for CNT growth with limited success with respect to quality and yield of CNTs (33, 34). Other synthesized Al hydroxide substrates were also used as catalyst support for CNT growth (35−37); however, in none of these cases were VA-CNTs obtained. Recently, work by Amama et al. has suggested that even the form of deposition of the same catalyst-support is significant to the catalyst and the CNT growth (38). Therefore, the contribution of the catalyst-suport alumina to VA-CNT growth is important and the development of an inexpensive approach that can reduce or eliminate its dependence on expensive catalyst-support deposition equipment and catalyst deposition techniques that are difficult to scale-up, has yet to be demonstrated.

In this work, we report a technique that overcomes the above difficulties by employing a completely liquid phase procedure for catalyst-support and catalyst deposition (Scheme 1). This technique is simple, cost-effective, and could be ideal for large-scale production of VA-CNT growth with further development. Premade Fe nanoparticles are used as catalysts on top of a thin film support made of alumoxane nanoparticles. The deposition is then performed through a simple spin-coating or dip-coating process, which makes the procedure competitive as a large-scale production technique.

## EXPERIMENTAL SECTION

Alumoxane solutions were prepared using boehmite particles (Catapal) from Sasol North America Inc., according to the procedure described by Callender et al. (39) Catapal (20 g) and [(methoxyethoxy)ethoxy]acetic acid (102 mL, 668 mmol) were heated to reflux in water (400 mL) for 72 h. The reaction mixture was centrifuged at 4400 rpm for 1 h. From this point forward, the decanted supernatant [(methoxyethoxy)ethoxy-]acetic acid mixture will be referred to as MEEA-alumoxanes (MEEA-A). The MEEA-A decant contains a large distribution of particle sizes. To separate the large particles, this solution was centrifuged at 29 000 rpm in a swing bucket ultracentrifuge (Discovery 100SE, Sorvall) for 12 h. The particle size was monitored by extracting aliquots of the MEEA-A and taking AFM images using tapping mode AFM (Digital Instruments, Nanoscope III Veeco Metrology Group, Santa Barbara, CA). Different concentrations of MEEA-A solution were tested by spin coating on clean $SiO_2$. The best concentration found was 0.015 mg/L for MEEA-A. Spin-coating this MEEA-A concentration at 4000 rpm produced good coverage films active in supporting VA-CNT growth. The alumoxane concentration in solution was determined by TGA. A volume of 0.1 mL of MEEA-A was dried in the oven at 100 °C, and the sample was then heated to 800 °C under Ar. The total remaining mass was 1.5 mg; therefore, the alumoxane concentration was 0.015 g/mL. Following the MEEA-A spin-coating, the substrates were immediately placed in the oven at 150 °C under a $N_2$ flow for 60 min. Film thickness measurements were determined with ellipsometry from 10 different spots in each sample, and measurement were done at 632 nm incident laser fixed at a 70° angle with 1.7 refraction index (Nf1) and Ns 385. Two catalyst cases were evaluated: In the first case, 0.5 and 1 nm films of Fe were deposited at $1 \times 10^{-6}$ Torr in an electron beam evaporator, whereas in the second case, the experiments were performed using 4.3 nm premade catalyst nanoparticles described below.

Unless noted otherwise, all chemicals were purchased from Sigma Aldrich and used as received. Premade catalyst nanoparticles were synthesized using a modified Sun method (40, 41) whereby Fe(III) acetylacetonate is reduced by excess 1,2-hexadecanediol in the presence of oleic acid and oleyl amine that form ligands on the particle surfaces. The reactants were added together at room temperature using benzyl ether as a solvent and brought to reflux under inert conditions for a period of 45 min. The particles were then precipitated using excess ethanol and repetitive centrifugation at 4000 rpm for 5 min. The precipitated particles were made soluble in hexanes and characterized as described below. The total concentration of Fe nanoparticles was determined with inductively coupled plasmon-atomic emission spectroscopy (ICP-AES) using a Perkin-Elmer optima 4300 DV, where the Fe concentration was found to be 40,000 ppm once the particles were synthesized and made soluble in approximately 15 mL of hexanes. The solution was then diluted in an iterative process to obtain maximal growth results by the further addition of hexanes. Once the optimal concentration was found for CNT growth, ICP-AES was carried out to determine the particle concentration. Initially, 100 $\mu$L of the optimal solution was digested in 500 $\mu$L of a 25% solution of hydrochloric acid with heating to digest the organic ligands; this was carried out twice. These metal particles were then digested in concentrated nitric acid overnight and diluted in nanopure water to carry out the ICP-AES. The sizes of the particles were found to be 4 nm as determined by small-angle X-ray scattering (SAXS) using a Rigaku SmartLab which correlated well with the 4.3 nm determined for the average particle size by AFM. The most successful nanoparticle concentration for growth of VA-CNTs was drop dried using 40−50 $\mu$L of a 0.128 mg/L solution of Fe. Assuming a 4 nm particle to contain 1300 Fe atoms, the particle concentration was calculated to be around $5.4 \times 10^{23}$ nanoparticles per liter.

CNT growth occurs in a water-assisted hot filament CVD reactor whose characteristics are detailed elsewhere (42, 43). In short, the evaporated films are reduced using atomic hydrogen for 30 s (produced from a hot filament) prior to growth, and in all cases, CNTs were grown for 15 min at 750 °C. In the case of the premade Fe nanoparticles, reduction was achieved

with 60 s of 10 mTorr $N_2H_4$ vapor exposure at 600 °C prior to growth (44). Growth takes place at 1.4 Torr in a 1 in. diameter tube furnace at 750 °C using a reaction gas mixture composed of $H_2O$ (2 standard cubic centimeters per second, (sccm)), $C_2H_2$ (2 sccm), and $H_2$ (410 sccm).

## RESULTS AND DISCUSSION

A crucial component of CNT growth by CVD is the catalyst-support, typically involving evaporated or sputtered $Al_2O_3$ thin films that support active metal catalyst such as Fe, Co, Ni, or combinations of these. Metal evaporation of films has several limitations, one being that it is a line-of-sight deposition technique and requires minimum pressures of $1 \times 10^{-5}$ Torr, making it time-consuming and difficult to scale. In addition, active particles in the CNT growth process typically form in the evaporation stage (44), meaning that any change in evaporation conditions can strongly perturb the resulting CNT growth. These limitations have a significant impact on VA-CNTs grown through a CVD process. Therefore, a reliable liquid phase method for catalyst and catalyst-support deposition represents a significant advance toward CNT mass production. Scheme 1 shows a pictorial presentation of the catalyst support, catalyst deposition procedure and the subsequent VA-CNT growth as we report in this work. The CNT growth was performed with evaporated catalyst film and premade catalyst nanoparticles.

Alumoxanes are nanoscale particles that are exfoliated from boehmite. These nanoparticles are dispersed in water through aluminum complexation by carboxylic acid ligands (39). Several varieties of carboxylic acids have been used to disperse alumoxanes in solution. We have previously shown that water dispersions of carboxylic-acid-functionalized alumina nanoparticles (carboxylate-alumoxanes) readily form continuous conformal 0.2−70 $\mu$m thick films on a wide range of substrates. The nanoparticles are converted to alumina upon mild thermolysis (45−47). Based upon our prior research, we have chosen to investigate MEEA-A for their film forming potential. We have selected MEEA ligands for our alumoxane studies based on the alumoxane stability in organic solvents, better dispersibility in solution, robustness to changes in pH and mainly stability of the dispersion toward aggregation at pH ~6 (48). There are several physical parameters of the MEEA-A we have explored in the past: we have documented the surface area, porosity, shrinkage as a function of alumoxanes fractional composition in films (49, 50), as well as other physical properties such as hardness, refractive index, and dielectric constants (39). We were able to develop and produce micrometer-thick substrates that would be suitable for micro electromechanical systems. Therefore, large surface coating of substrates with this technique is not new. However, in prior studies, the surface continuity and nanoscale surface smoothness were not required; therefore, ultracentifuging of alumoxane solutions was not necessary.

MEEA-A as-prepared, before ultracentrifugation, has a broad distribution of particle sizes with many as large as 12.7 nm as determined by AFM characterization, even after 1 (Figure 1a) and 3 h of ultracentrifugation. To facilitate alumoxane thin film deposition relevant to VA-CNT growth,

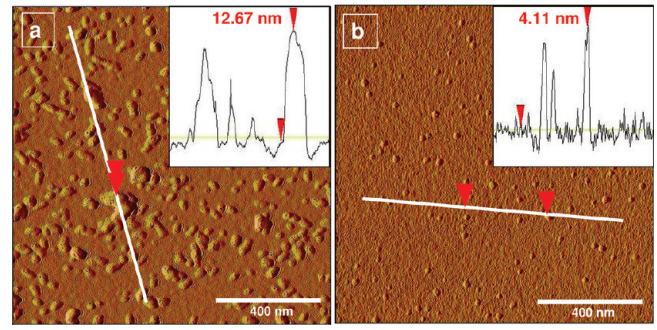


**FIGURE 1. AFM images of the alumoxanes nanoparticles after (a) 1 and (b) 12 h of ultracentrifugation at 29 000 rpm. After 1 h of ultracentrifugation, particles with heights as high as 12.7 nm were recorded, and after 12 h of ultracentrifugation, only particles below 4.1 nm shown in AFM figure were observed.**

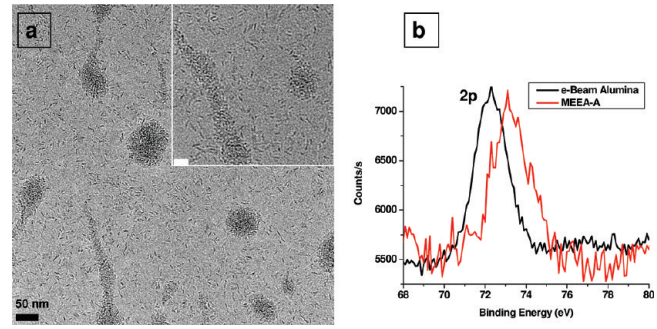


**FIGURE 2. (a) TEM images of MEEA-A nanoparticles after 12 h of ultracentrifugation revealing rodlike structures; notice the very small structures of rods in the TEM inset, scale bar 20 nm. (b) XPS of the thin film prepared with MEEA-A through spin coating. The Al signal of the MEEA-A thin film was multiplied by 3.15 to achieve the same signal intensity as the evaporated 10 nm $Al_2O_3$.**

we removed large particles from solution by 12 h ultracentrifugation. As evidenced by AFM images in Figure 1b, most of the large particles precipitate after 12 h at 29 K RPM. The supernatant solution is found to only contain particles smaller than ~4.1 nm in suspension, suggesting a narrower size distribution. These small nanoparticle distributions reveal rod-like structures as seen by transmission electron microscopy (TEM), Figure 2a. The use of these smaller alumoxane particles in catalyst support preparation for VA-CNT growth allows the film roughness to be similar to conventional evaporated or sputtered $Al_2O_3$ (rms = ~0.7 nm). The thickness of the film was determined using ellipsometry from two different films prepared with similar procedures with measurements from 10 random spots on each film. These measurements yield a thickness of 10.3 ± 2.1 nm, and 8.8 ± 1.0 nm. The MEEA-A film characterized by X-ray photoelectron spectroscopy (XPS) supports the formation of an alumina coating; however, the signal intensity is ca. 3 times smaller than that of evaporated $Al_2O_3$ of similar film thickness as seen in Figure 2b. Considering that the MEEA-A is a film made completely from nanoparticles, it is expected to have higher porosity and lower density compared to evaporated $Al_2O_3$.

Spin-coating 200 $\mu$L of the 0.015 g/mL MEEA-A solution gave a uniform coating on a ~4 $cm^2$ square $SiO_2$ surface. The uniform coating is evidenced by the VA-CNTs that grew on the surface and shown in Figure 3a. Conversely, the same

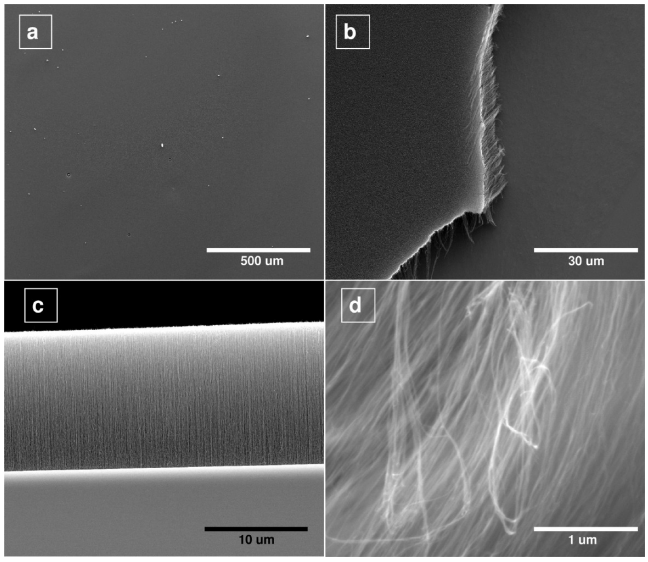


**FIGURE 3. SEM images of VA-CNTs grown from Fe evaporated catalyst on MEEA-A thin films as catalyst support (0.015 g/mL). (a) View of top surface of CNTs. (b) VA-CNT view through an open area. (c) Side view of the VA-CNTs to measure the height of the forest. (d) closer view of CNTs.**

volume of 0.005 and 0.025 g/mL solutions leave a nonuniform islanded surface morphology (see the Supporting Information). Any unevenness of the alumoxane-derived film results in an equivalent nonuniformity of the VA-CNT growth such that for 0.005 and 0.025 g/mL solutions, the CNT heights were uneven with some areas significantly taller than others. This suggests that film uniformity is important in ensuring uniform carpet growth. Furthermore, in the case of the more concentrated MEEA-A solutions (0.025 g/mL), areas of the film can be as thick as 500 nm and were found to peel off during the CNT growth process. It is surprising that a small change in the concentration significantly affects the homogeneity of films, considering that film preparation from a colloidal nanoparticle solution has a complex contribution from many parameters such as capillary effects, electrostatic charges, density and viscosity of the solvents. The density of MEEA (1.16 g/mL) is relatively higher and the solution appears to be more viscous than water. Film formation seems to be determined by capillary forces interacting between the solvent and the substrate. Possibly local higher particle concentration that develops during drying can change the mobility of the remaining particles in the solution therefore changing capillary forces to favor particle aggregation.

The hygroscopic nature of MEEA-A requires that after spin-coating the samples should be dried in a water-free environment. The samples were immediately placed in a $N_2$-purged oven at 150 °C, and the solvent was allowed to evaporate for 60 min. This was found to be an important post-film-making step to guarantee surface planarity of the film. In cases where drying was not performed, we have observed that within a few minutes, a uniform film loses its surface uniformity and creates agglomerates or aggregates that distort the planarity of the substrate.

Iron catalyst was deposited on the alumoxane-derived substrates by two methods. For the evaporated catalyst, 0.5 and 1 nm of iron deposition was performed at $1 \times 10^{-6}$ Torr in an electron beam evaporator. As is shown in Figure 3b–d, the quality of the CNTs growth by SEM is similar to that of CNTs grown on evaporated $Al_2O_3$ substrates. The height of the VA-CNT is 17 $\mu$m (Figure 3c) for a 15 min growth duration, which is slightly lower than, but comparable to, the ~20 $\mu$m achieved by using the same conditions on single-crystal $Al_2O_3$. However, this is shorter than CNTs grown on evaporated $Al_2O_3$ (~40 $\mu$m).

As a matter of comparison and to assess the importance of the alumoxane film for CNT growth, we have performed a control experiment whereby a $SiO_2$ substrate with no alumoxane film and another with a MEEA-A film, were coated at the same time with electron beam evaporated Fe catalyst. Both substrates were placed in the CVD reactor for a 15 min CNT growth period. As expected, both substrates grew CNTs; however, the $SiO_2$ substrate grew only a small amount of CNTs on the surface, whereas the MEEA-A substrate produced a homogeneous carpet of VA-CNTs across the entire surface. TEM images of VA-CNTs grown on alumoxane substrates from evaporated catalyst indicate a variety of diameters and small number of walls (Figure 4a). Typically, the CNTs are 3–7 nm in diameter and often are composed of double- and triple-walled CNTs; Raman spectroscopy reveals the presence of some smaller diameter single-walled CNTs (Figure 4b) present among the larger ones. Laser excitations at 514, 633, and 785 nm wavelengths detect radial breathing modes (RBM) between 300–100 $cm^{-1}$ typical of CNTs with diameters 2.5 to 0.7 nm. The same is observed in VA-CNTs grown on evaporated $Al_2O_3$. The D/G ratio, which is an indication of quality based on defects in the CNT, are 18, 21 and 29% for 514, 633, and 785 nm excitations, respectively.

Besides the deposition of catalyst-support by a liquid phase method, as we have discussed thus far, metal catalyst deposition through a liquid process allows for a completely scalable technique for catalyst and catalyst support deposition. Ideally, a dense, yet submonolayer coating of uniformly spaced premade Fe particles on a catalyst support will grow a homogeneous layer of aligned CNTs. For iron catalyst deposition from premade nanoparticles, we have used two approaches to construct layers of particles for CNT growth using both spin coating and drop drying. Spin coating is an effective way to deposit thin layers of particles even though this technique is sensitive to particle concentration in solution, spinning speed and other properties related to the solvent. To mitigate the formation of patches of particles during drying, we found that drop evaporation of 40–50 $\mu$L of particle solution was effective in making uniform semimonolayers of particles. When this was combined with catalyst nanoparticle reduction by $N_2H_4$, high-quality VA-CNTs (Figure 5a) were grown.

In the CVD growth of VA-CNTs, a critical factor in achieving controllable growth and scalability is the reduction of the catalyst layer. This has been addressed by some of us where $N_2H_4$ vapor was used to reduce evaporated metal catalysts with brief exposures at lower than growth temperatures (44).

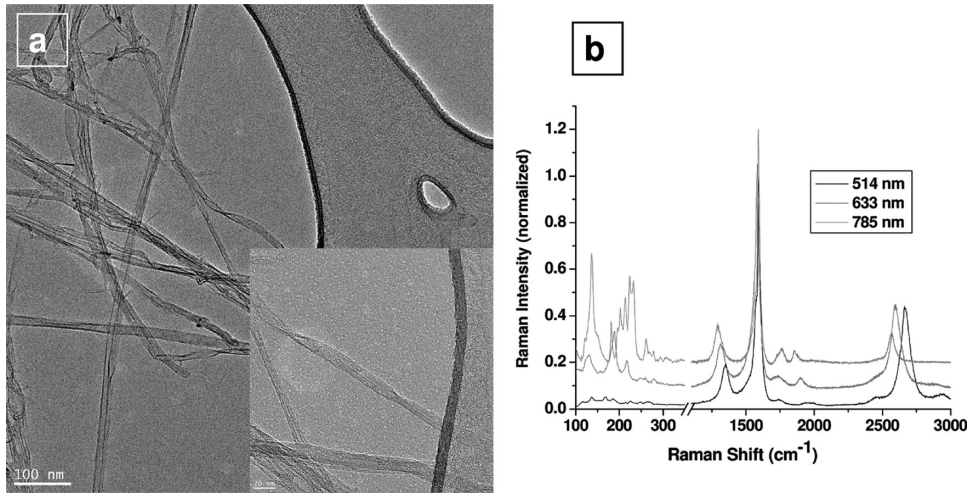


FIGURE 4. (a) TEM images of CNTs grown from electron beam evaporated catalyst on MEEA-A thin films as catalyst support (inset scale bar 20 nm). (b) Raman spectra of VA-CNTs grown from evaporated Fe catalyst on MEEA-A thin film catalyst support.

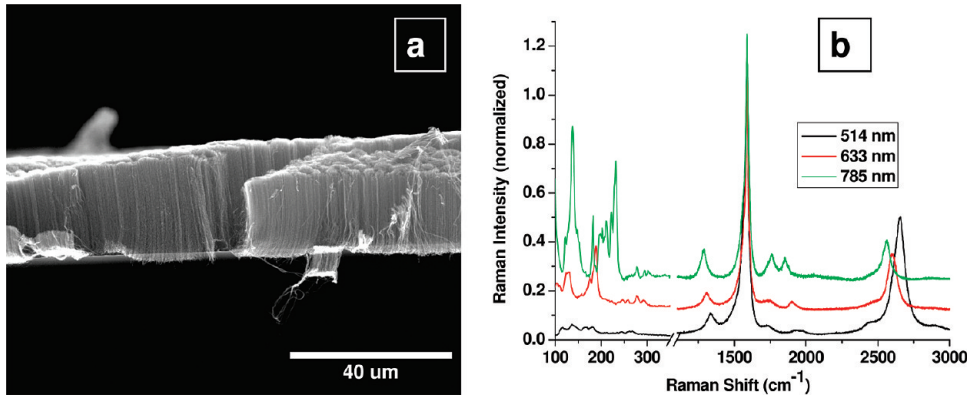


FIGURE 5. (a) SEM image and (b) Raman spectra of VA-CNTs grown from premade 4.3 nm Fe nanoparticles on MEEA-A thin film catalyst support.

$N_2H_4$ reduction has several advantages compared with hot filament reduction that operates based on the generation of atomic hydrogen or the use of reduction with molecular hydrogen. The use of $N_2H_4$ avoids complications of the dimension and geometries of a filament required in order to evenly reduce the particles on surfaces, especially for large surface area supports, and allows catalyst reduction at lower temperatures than hydrogen. $N_2H_4$ reduction of our premade Fe nanoparticles has proven to be efficient and robust and the probability of hidden or nonreduced catalyst areas is much smaller. The Raman spectra of the CNTs grown from premade Fe nanoparticles (Figure 5b) combined with $N_2H_4$ reduction shows features that are similar to the CNTs grown from evaporated Fe on MEEA-A. A liquid phase approach to metal catalyst/catalyst support deposition combined with $N_2H_4$ vapor reduction allows VA-CNT growth via CVD to be suitable for scale-up. In addition, the use of $N_2H_4$-based low temperature reduction of catalyst particles means that reduction can take place efficiently and leads to nucleation of CNT in the growth reactor before particle coarsening begins to occur. Recently, control of coarsening has been shown to be a critical factor in determining the growth quality of VA-CNTs (51). Thus a liquid phase process to deposit catalyst-support and catalyst on a surface leads to high-quality VA-CNT growth in a scalable manner.

## CONCLUSION

A simple and scalable route for CNT production by CVD has been developed. The approach is based on a complete liquid phase deposition process of catalyst and catalyst support. Through simple changes in concentration, we deposited homogeneous thin films of alumoxane nanoparticles that have comparable continuity and smoothness to evaporated $Al_2O_3$ and yield CNTs with similar characteristics. Additionally, premade catalyst particles were deposited on alumoxanes films and high-quality CNTs were grown. Premade catalyst particle reduction using $N_2H_4$ lifts the barriers of reduction and sample preparation in a CVD process to yield a facile technique that can be adapted as a large-scale CNT production.

**Acknowledgment.** The authors thank Sasol North America for providing aluminas and Carter Kitrell for helpful discussions. This work was supported by the Air Force Research Laboratories under Contract FA8650-05-D-5807, the Air Force Office of Scientific Research FA9550-09-1-0581, and PrivaTran, LLC, through the SBIR program via the Army Research Office.

**Supporting Information Available:** SEM images of VA-CNTs grown using different concentrations of MEEA-A (PDF).

This material is available free of charge via the Internet at http://pubs.acs.org.

## REFERENCES AND NOTES


(1) Dresselhaus, M. S.; Dresselhaus, G.; Avouris, P. *Carbon Nanotubes Synthesis, Structure, Properties and Applications*; Springer-Verlag: Berlin, Germany, 2001.
(2) Saito, R.; Dresselhaus, G.; Dresselhaus, M. S. *Physical Properties of Carbon Nanotubes*; Imperial College Press: London, 1998.
(3) Rutherglen, C.; Burke, P. *Nano Lett.* **2007**, *7*, 3296–3299.
(4) Jensen, K.; Weldon, J.; Garcia, H.; Zettl, A. *Nano Lett.* **2007**, *7*, 3508–3511.
(5) Xiao, L.; Chen, Z.; Feng, C.; Liu, L.; Bai, Z.-Q.; Wang, Y.; Qian, L.; Zhang, Y.; Li, Q.; Jiang, K.; Fan, S. *Nano Lett.* **2008**, *8*, 4539–4545.
(6) Jung, S. M.; Jung, H. Y.; Suh, J. S. *Carbon* **2008**, *46*, 1973–1977.
(7) Rakhi, R. B.; Sethupathi, K.; Ramaprabhu, S. *Carbon* **2008**, *46*, 1656–1663.
(8) Pushparaj, V. L.; Shaijumon, M. M.; Kumar, A.; Murugesan, S.; Ci, L.; Vajtai, R.; Linhardt, R. J.; Nalamasu, O.; Ajayan, P. M. *Proc. Natl. Acad. Sci. U.S.A.* **2007**, *104*, 13574–13577.
(9) Chou, S.; Wang, J.; Chew, S.; Liu, H.; Dou, S. *Electrochem. Commun.* **2008**, *10*, 1724–1727.
(10) Nikolaev, P.; Bronikowski, M. J.; Bradley, R. K.; Rohmund, F.; Colbert, D. T.; Smith, K. A.; Smalley, R. E. *Chem. Phys. Lett.* **1999**, *313*, 91–97.
(11) Wei, F.; Zhang, Q.; Qian, W.; Yu, H.; Wang, Y.; Luo, G.; Xu, G.; Wang, D. *Powder Technol.* **2008**, *183*, 10–20.
(12) Zhang, Q.; Zhao, M.-Q.; Huang, J.-Q.; Liu, Y.; Wang, Y.; Qian, W.-Z.; Wei, F. *Carbon* **2009**, *47*, 2600–2610.
(13) Zhang, Q.; Zhao, M.-Q.; Huang, J.-Q.; Nie, J.-Q.; Wei, F. *Carbon* **2010**, *48*, 1196–1209.
(14) Zhang, Q.; Zhao, M.; Liu, Y.; Cao, A.; Qian, W.; Lu, Y.; Wei, F. *Adv. Mater.* **2009**, *21*, 2876–2880.
(15) Xiang, R.; Luo, G.; Qian, W.; Wang, Y.; Wei, F.; Li, Q. *Chem. Vap. Deposition* **2007**, *13*, 533–536.
(16) Xiang, R.; Luo, G.; Yang, Z.; Zhang, Q.; Qian, W.; Wei, F. *Mater. Lett.* **2009**, *63*, 84–87.
(17) Feng, C.; Liu, K.; Wu, J.-S.; Liu, L.; Cheng, J.-S.; Zhang, Y.; Sun, Y.; Li, Q.; Fan, S.; Jiang, K. *Adv. Funct. Mater.* **2010**, *20*, 885–891.
(18) Zhang, M.; Atkinson, K. R.; Baughman, R. H. *Science* **2004**, *306*, 1358–1361.
(19) Ren, L.; Pint, C. L.; Booshehri, L. G.; Rice, W. D.; Wang, X.; Hilton, D. J.; Takeya, K.; Kawayama, I.; Tonouchi, M.; Hauge, R. H.; Kono, J. *Nano Lett.* **2009**, *9*, 2610–2613.
(20) Pint, C. L.; Pheasant, S. T.; Pasquali, M.; Coulter, K. E.; Schmidt, H. K.; Hauge, R. H. *Nano Lett.* **2008**, *8*, 1879–1883.
(21) Harutyunyan, A. R. *J. Nanosci. Nanotechnol.* **2009**, *9*, 2480–2495.
(22) Nishino, H.; Yasuda, S.; Namai, T.; Futaba, D. N.; Yamada, T.; Yumura, M.; Iijima, S.; Hata, K. *J. Phys. Chem. C* **2007**, *111*, 17961–17965.
(23) Franklin, N. R.; Li, Y.; Chen, R. J.; Javey, A.; Dai, H. *Appl. Phys. Lett.* **2001**, *79*, 4571–4573.
(24) Murakami, Y.; Chiashi, S.; Miyauchi, Y.; Hu, M.; Ogura, M.; Okubo, T.; Maruyama, S. *Chem. Phys. Lett.* **2004**, *385*, 298–303.
(25) Méhn, D.; Fonseca, A.; Bister, G.; Nagy, J. B. *Chem. Phys. Lett.* **2004**, *393*, 378–384.
(26) Liu, J.; Li, X.; Schrand, A.; Ohashi, T.; Dai, L. *Chem. Mater.* **2005**, *17*, 6599–6604.
(27) Ciambelli, P.; Sannino, D.; Sarno, M.; Fonseca, A.; Nagy, J. B. *Carbon* **2005**, *43*, 631–640.
(28) Vander Wal, R. L.; Hall, L. J. *Carbon* **2003**, *41*, 659–672.
(29) Ohno, H.; Takagi, D.; Yamada, K.; Chiashi, S.; Tokura, A.; Homma, Y. *Jpn. J. Appl. Phys.* **2008**, *47*, 1956–1960.
(30) Kocabas, C.; Kang, S. J.; Ozel, T.; Shim, M.; Rogers, J. A. *J. Phys. Chem. C* **2007**, *111*, 17879–17886.
(31) Yoshikawa, N.; Asari, T.; Kishi, N.; Hayashi, S.; Sugai, T.; Shinohara, H. *Nanotechnology* **2008**, *19*, 1–5.
(32) Hiraoka, T.; Yamada, T.; Hata, K.; Futaba, D. N.; Kurachi, H.; Uemura, S.; Yumura, M.; Iijima, S. *J. Am. Chem. Soc.* **2006**, *128*, 13338–13339.
(33) Aghababazadeh, R.; Mirhabibi, A. R.; Ghanbari, H.; Chizari, K.; Brydson, R. M.; Brown, A. P. *J. Phys.: Conf. Ser.* **2006**, *26*, 135–138.
(34) Ciambelli, P.; Sannino, D.; Sarno, M.; Leone, C.; Lafont, U. *Diamond Relat. Mater.* **2007**, *16*, 1144–1149.
(35) Nagaraju, N.; Fonseca, A.; Konya, Z.; Nagy, J. B. *J. Mol. Catal. A: Chem.* **2002**, *181*, 57–62.
(36) Kathyayini, H.; Willems, I.; A., F.; Nagy, J. B.; Nagaraju, N. *Catal. Commun.* **2006**, *7*, 140–147.
(37) Hongo, H.; Nihey, F.; Ichihashi, T.; Ochiai, Y.; Yudasaka, M.; Iijima, S. *Chem. Phys. Lett.* **2003**, *380*, 158–164.
(38) Amama, P. B.; Pint, C. L.; Kim, S. M.; McJilton, L.; Eyink, K. J.; Stach, E. A.; Hauge, R. H.; Maruyama, B. *ACS Nano* **2010**, *4*, 895–904.
(39) Callender, R. L.; Harlan, C. J.; Shapiro, N. M.; Jones, C. D.; Callahan, D. L.; Wiesner, M. R.; MacQueen, D. B.; Cook, R.; Barron, A. R. *Chem. Mater.* **1997**, *9*, 2418–2433.
(40) Sun, S.; Zeng, H. *J. Am. Chem. Soc.* **2002**, *124*, 8204–8205.
(41) Crouse, C. A.; Barron, A. R. *J. Mater. Chem.* **2008**, *18*, 4146–4153.
(42) Pint, C. L.; Pheasant, S. T.; Parra-Vasquez, A. N. G.; Horton, C.; Xu, Y.; Hauge, R. H. *J. Phys. Chem. C* **2009**, *113*, 4125–4133.
(43) Xu, Y.; Flor, E.; Kim, M. J.; Hamadani, B.; Schmidt, H.; Smalley, R. E.; Hauge, R. H. *J. Am. Chem. Soc.* **2006**, *128*, 6560–6561.
(44) Pint, C. L.; Kim, S. M.; Stach, E. A.; Hauge, R. H. *ACS Nano* **2009**, *3*, 1897–1905.
(45) Callender, R. L.; Barron, A. R. *J. Mater. Res.* **2000**, *15*, 2228–2237.
(46) Callender, R. L.; Barron, A. R. *J. Mater. Sci.* **2001**, *36*, 4977–4987.
(47) Loscutova, R.; Barron, A. R. *J. Mater. Sci.* **2006**, *41*, 3391–3401.
(48) Vogelson, C. T.; Barron, A. R. *J. Non-Cryst. Solids* **2001**, *290*, 216–223.
(49) Jones, C. D.; Barron, A. R. *Mater. Chem. Phys.* **2007**, *104*, 460–471.
(50) Bailey, D. A.; Jones, C. D.; Barron, A. R.; Wiesner, M. R. *J. Membr. Sci.* **2000**, *176*, 1–9.
(51) Amama, P. B.; Pint, C. L.; McJilton, L.; Kim, S. M.; Stach, E. A.; Murray, T. M.; Hauge, R. H.; Maruyama, B. *Nano Lett.* **2009**, *9*, 44–49.


AM100128M